The Effect of Shape and Density on the Free Settling of Particles at High Reynolds Numbers

E. B. CHRISTIANSEN and DEE H. BARKER

University of Utah, Salt Lake City, Utah

Terminal velocity drag coefficients C_D were determined for cylinders, prisms, disks, and spheres in air and water at N_{Re} from 1,000 to 300,000, the regime where particles rotate and/or oscillate. These and other similar data show that C_D is a function of particle and fluid densities ρ_p and ρ_f, as well as shape and N_{Re}.

By considering C_D a function of particle moment of inertia and the rotational moment generated by circulation (or alternatively the field force and the lift), one can deduce that $C_D = f\left(\frac{\rho_p}{\rho_f}$ or $\frac{\rho_p - \rho_f}{\rho_f}$, a length ratio, $N_{RE}\right)$. This relationship correlates the data for $\rho_p = 1.2$ to 8.3 and $\rho_f = 0.1$ to 1.3 g./cc. to within $\pm$ 10%.

Data on the fluid dynamic forces acting on bodies moving through fluids are of importance in the design and operation of chemical process equipment such as crystallizers, classifiers, centrifuges, dust collectors, pneumatic and hydraulic conveyors, and rocket engines.

It would be desirable, given the shape and physical properties of a particle, the physical properties of the fluid, and the magnitude and direction of the force field, to be able to predict the motion of the particle by use of equations or graphs. This goal has been partially attained.

It has been shown both theoretically and experimentally that, if fluid compression is negligible, the resisting force R acting on a body moving freely in a fluid depends on the velocity of the body relative to the fluid u, an area A, the fluid density ρ_f, and the fluid viscosity μ. The area and velocity are usually arbitrarily chosen as the projected area and the relative velocity in the direction of the force field. By dimensional analysis and after the arbitrary substitution of $u^2\rho_f/2$ for $u^2\rho_f$, the following relationship for these variables can be obtained (*13*):

$$\frac{2R}{A\,\rho_f\,u^2} = f\frac{(du\rho_f)}{\mu} \qquad (1)$$

The exact function f is complicated and usually presented by plotting experimental values for the drag coefficient C_D [the dimensionless group of the left side of Equation (1)] vs. the Reynolds number N_{Re} on log-log graph paper. In the case of steady state free fall in a gravitational force field

$$R = V(\rho_p - \rho_f)g \qquad (2)$$

Numerous free settling rate data have been collected for spherical bodies and, in general, it has been possible to represent these data by a single, continuous curve by plotting C_D vs. N_{Re}, usually on log-log paper (*19*). Extensive data, C_D vs. N_{Re} curves, and a useful correlation have been reported for isometric particles including spheres, cubes, octahedrons, cube octahedrons, and tetrahedrons for laminar flow conditions ($Re > 0.05$), transitional flow conditions (N_{Re} from 0.05 to about 100 to 1,000 depending on particle shape), and for turbulent flow conditions to $N_{Re} = 22{,}000$ (*3, 20*).

Data and useful correlations for laminar free fall of various cylinders and rectangular parallelepipeds have been reported by Heiss and Coull (*10*). Additional nonisometric particle research for both laminar and transitional flow conditions has been reported [for example (*4, 11, 17, 22, 23*)]. However, attempts to develop generalized correlations for nonisometric particles under transitional flow conditions have not been entirely successful.

In the case of more or less turbulent flow ($N_{Re} > 100$ to 1,000, depending on particle shape) the previously published free settling data for well-defined, nonisometric particles are limited to those reported by Duplieh (*9*) for plates and some three-dimensional shapes in air and water, by Pernolet (*18*) and Krumbein (*12*) for particles of only one volume and density but of varying shape settling in water, by Willmarth et al. (*26*) for disks, and a few other restricted sets of data. Considerably more data are necessary for correlation work, particularly in light of the observation that in turbulent flow, data for isometric and especially nonisometric particles of identical shape but of different density do not have the same $C_D - N_{Re}$ relationship (*5, 8*).

The objective of the presently reported research is to provide additional turbulent flow data on well-defined, nonisometric particles and to develop a correlation of variables more generally applicable to turbulent flow conditions than the previously developed relationships.

EXPERIMENTAL APPARATUS AND PROCEDURE

Free settling rates for disks, prisms, and spheres of several densities in water and, to a limited extent, in air were determined.

The Particles

It was felt that previously published turbulent flow data for spheres and isometric shapes in water and similar fluids were adequate for use in correlation studies but that the few available data on prisms and disklike particles were inadequate. Therefore, families of particles were manufactured which had round, hexagonal, square, and equilateral triangular cross sections and which varied in length (height) from flat shapes (disks) which had height to diameter ratios of $\sim$ 0.2 to 0.6 to long shapes (cylinders and prisms) which had length to diameter ratios of $\sim$ 1.5 to 6.0. Diameters varied from 0.2 to 2.54

Dee H. Barker is at Brigham Young University, Provo, Utah.

TABLE 1. EXPERIMENTAL RESULTS IN AIR*

d, (cm.)	d_{Re}, (cm.)	Material	N	u, (cm./sec.)	N_{Re}	$\frac{\rho_p}{\rho_f}$	C'_D, Equation (5)	$\frac{\rho_p - \rho_f}{\rho_f}$	C'_D, Equation (4)
				Spheres ($\Psi = 1.000$)					
0.9523	0.9523	Aluminum	4	2,869	15,030	2,796	0.480	2,795	0.536
1.547	1.547	Lucite	1	2,394	20,370	1,178	0.465	1,177	0.513
				Cylinders ($\Psi = 0.846$, $L/d = 1.75$)					
1.27	2.223	Aluminum	1	2,880	35,320	2,783	0.997	2,872	0.975
1.11	1.946	Aluminum	1	2,751	29,440	2,801	0.962	2,800	0.940
0.795	1.389	Aluminum	2	2,349	17,950	2,774	0.936	2,773	0.915
0.635	1.340	Aluminum	1	2,150	13,040	2,773	0.892	2,772	0.872
1.875	3.380	Magnesium	3	2,711	50,400	1,776	1.037	1,775	1.014
1.278	2.352	Magnesium	1	2,425	31,370	1,806	0.936	1,805	0.879
1.102	1.923	Magnesium	1	2,304	24,370	1,827	0.864	1,871	0.872
0.648	1.102	Magnesium	1	1,648	9,989	1,750	0.955	1,749	0.933
2.520	5.480	Lucite	1	2,560	80,470	1,178	1.012	1,177	0.993
1.897	3.330	Lucite	1	2,194	40,180	1,177	1.032	1,176	1.014
1.257	2.250	Lucite	1	1,914	23,690	1,178	0.902	1,177	0.886
				Round disk ($\Psi = 0.806$, $d_{min}/d_{max} = 0.603$, height/$d = 0.225$)					
1.095	1.095	Magnesium	1	1,545	9,305	1,016	1.25	1,815	1.221

* $\rho_f = 1 \times 10^{-3}$ g./cc.
$\mu = 0.0182 \times 10^{-2}$ poise

cm. To facilitate comparison of the new data with existing well-defined data (*5, 8*), these nonisometric particles were manufactured, where possible, with sphericities Ψ of 0.906, 0.846, 0.806, and 0.67. Particles having a maximum sphericity for each cross section were also manufactured. The surfaces of manufactured particles were polished with fine emery cloth. Steel, aluminum, and Lucite spheres were obtained principally for evaluation of experimental procedures.

The particles were manufactured from materials having a wide range of densities: brass, steel, titanium, aluminum, magnesium, and Lucite. In general, a set of two or more specimens for each size, length, or height to diameter ratio, cross-sectional shape, and density were manufactured.

Particle densities were calculated from the weight in air and in water and are accurate to within four significant figures. Density accuracy is more important in the case of the Lucite particle data where, owing to density inaccuracy, a maximum error in the value of C_D of less than 1% may have been introduced.

The Settling Columns

A settling tank, 4 ft. in diameter and 15 ft. high, was used in obtaining the free-fall data in water. Three horizontal plate-glass observation windows, 3 in. high by 2 ft. long, were provided at heights of 1, 5, and 8-ft. from the bottom of the tank. Above each observation window, a plate-glass window 6 in. sq. was provided for illumination.

The free-fall determinations in air were made in an unused smokestack at Murray, Utah. This stack is 455 ft. tall, about 40 ft. I.D. at the base, and about 22 ft. I.D. at the top. The top was sealed.

Fluid Properties

Fluid densities and viscosities for water and air corresponding to the experimental temperatures were taken from the "Handbook of Chemistry and Physics." No effort was made to keep the water temperature constant, but it was found to vary no more than about 1°C. over several days time. The temperature gradient between the top and the bottom of the tank was negligible.

The temperature gradient for the air in the smokestack, as determined by means of thermocouples located 30 and 75 ft. above the floor of the smokestack, was less than 0.5°C.

Settling Velocity Determination

Most of the velocity determinations were made by use of a photoelectric timer (*1, 6*) wherein reflected light from a falling particle is detected at two different levels by photoelectric cells whose output started and stopped a timing device. The maximum absolute but random timing error in a photoelectric timing observation was about 0.017 sec. The Lucite particles and a few other slow-settling particles, for which timing intervals of 0.5 to 6 sec. were possible, were timed by means of a stop watch, as is indicated in the data tables of reference *1*.

About ten duplicate free-fall observations were made in water to reduce the probable error in the average observed-time interval. Particles of a few sets usually struck the column wall while falling, and in these cases it was impractical to obtain many free-fall determinations. Also, owing to experimental difficulties, only one to four free-fall determinations for each particle were made in air. In air tests, the timer did not respond consistently to the light reflected from the smaller particles, and, with the exception of the spheres, the low-density particles usually wandered outside the timing light beam in their descent.

As a check on the attainment of steady state velocities, particles were timed in water after free falls of both 225 and 300 cm. and in air after free falls of 350 and 400 ft. It was established that, in water experiments, the particles reached steady state velocities before entering the upper timing plane. Timing data indicate that the larger and the higher density particles did not attain steady state velocities in air in the free-fall distance available.

EXPERIMENTAL RESULTS

The numerous experimental data for water (analogous to those for air presented in Table 1 herein) are recorded in Tables 8 and 9 of references *1, 7, 27*. Data for particles which probably attained at least 95% of the steady state velocity in air are presented in Table 1. In support of the accuracy of the measurements, most of the velocity data for spheres in water are within ± 3% of those calculated (*1*) by means of the usually accepted C_D vs. N_{Re} data (*19*).

Particle behavior during free fall, an important factor in flow resistance, varies with N_{Re}, particle shape, and at high N_{Re} particle behavior is also influenced by particle density. The effect of particle moment of inertia, which is derived from particle geometry and density, on particle behavior and drag coefficients at high N_{Re} (1) is emphasized in this study. Under transitional flow conditions (for nonspherical particles $N_{Re} \cong 0.1$ to 100 to 600 depending

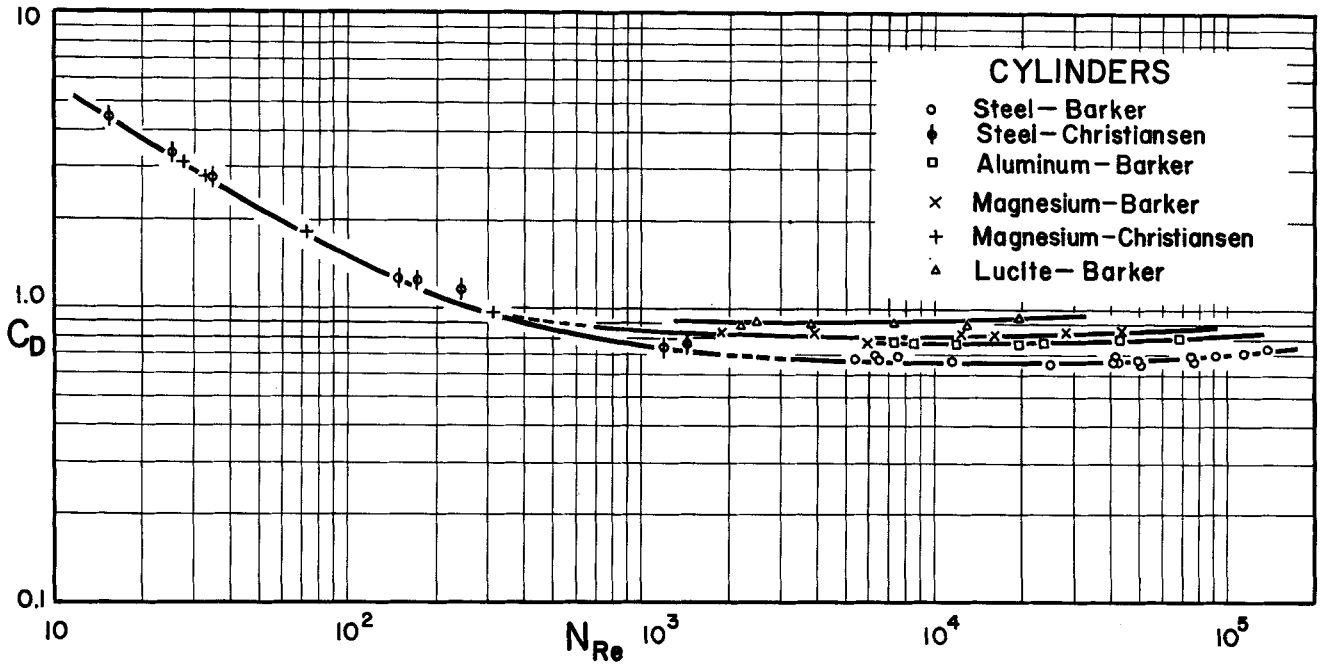

Fig. 1. C_D vs. N_{Re} for cylinders of various densities in water (Barker) and in aqueous glucose (Christiansen). (L/d = 2.5, ψ = 0.806).

on shape), particles fall, oriented with the largest flat surface (the largest projected area in the case of cylinders) perpendicular to the direction of motion (*1, 4, 5, 8*). However, in the range of N_{Re} of ~ 100 to 10^5, where the particle wake is increasingly turbulent, disks or plates (round, hexagonal, square, and triangular) oscillated about the longest (usually horizontal) axis as they fell with a zig-zag motion or spun along a somewhat helical path, depending on the moment of inertia and N_{Re}. The dependence of the behavior of very thin circular disks on the moment of inertia and N_{Re} has also been investigated by Willmarth et al. (*26*). In this high N_{Re} range, prisms rotated around the long (approximately horizontal) axis and descended along a nonvertical and frequently helical path. A helical descent rather than a straight descent at an angle with the vertical may have been a consequence of a lack of exact particle symmetry in some cases. The cylinders appeared to fall like the prisms except at the higher N_{Re} where they oscillated (teetered) about the center of gravity; however, spin on the long axis was not directly observed, and deviation from a vertical path was less than in the case of prisms. Isometric and approximately isometric particles rotated or spun and descended along a helical path. [Although spheres fell along a slightly spiral path, as previously predicted and observed (*5, 16*), it was not ascertained whether or not they spun.] For a specific shape, the deviation from a vertical path was less the higher the particle density. These patterns of motion were observed in air as well as in water in the N_{Re} range of ~ 300 to 10^5.

If, after the particle has reached steady state free-fall conditions in the N_{Re} range of ~ 300 to 10^5, instantaneous velocities are continuously measured over a single oscillation or rotation cycle, both the angular and translation velocities are observed to vary (*9*). The steady state free-fall velocity of spheres has also been observed to be periodic at high values of N_{Re} (*5, 14, 22*).

CORRELATION OF DATA

The data of this investigation for nonisometric particles, maximum-sphericity particles, and spheres in water and air (*1*), previously published isometric particle data (*5, 20*), some data from a previous investigation (*8*) for nonisometric particles in aqueous glucose solutions, some data for nonisometric particles in a hydrocarbon oil (*4*), and the data of Lunnon for spheres in air were used in correlation studies.

Preliminary calculations indicated that inflections in the C_D vs. N_{Re} data plots would occur more nearly at the same N_{Re} for all shapes if the length used in calculating the N_{Re} was the length of the cylinder or prism, or the longest line in the cross section of the disks. Hence, these lengths were used in calculating N_{Re}. In the case of the maximum sphericity and isometric shapes, the spherical diameter was used in computing N_{Re}.

The area of the flat face of disks and the maximum projected area in a plane parallel to the long axis of the cylinders and prisms were used in Equation (1). In the case of isometric and maximum-sphericity particles, the projected area of the sphere having the same volume as that of the particle was used.

Values of C_D are plotted vs. N_{Re} in Figure 1 for geometrically similar steel, aluminum, magnesium, and Lucite cylinders having a sphericity of 0.806 settling in water and in aqueous glucose solution. The lines drawn through the data for 0.806 sphericity cylinders in Figure 1 represent equally well the analogous data for 0.846 sphericity cylinders.

It is apparent from an examination of Figure 1 that in the N_{Re} range of ~ 300 to 10^5, where particles rotate or oscillate, the drag coefficient decreases with increase in particle density as has been suggested by earlier studies (*2, 5, 8, 21*). However, at lower Reynolds numbers where the particles do not rotate or oscillate, all of the points fall on a single line independent of the density of the particle. A similar drag coefficient-density dependency in the N_{Re} range of ~ 300 to 10^5 was observed in the case of all particle shapes studied.

This drag coefficient-density dependency is evidently related to particle rotation and/or oscillation; furthermore, particle oscillation and rotation are associated with the periodic growth and shedding of eddies (*22*). For each

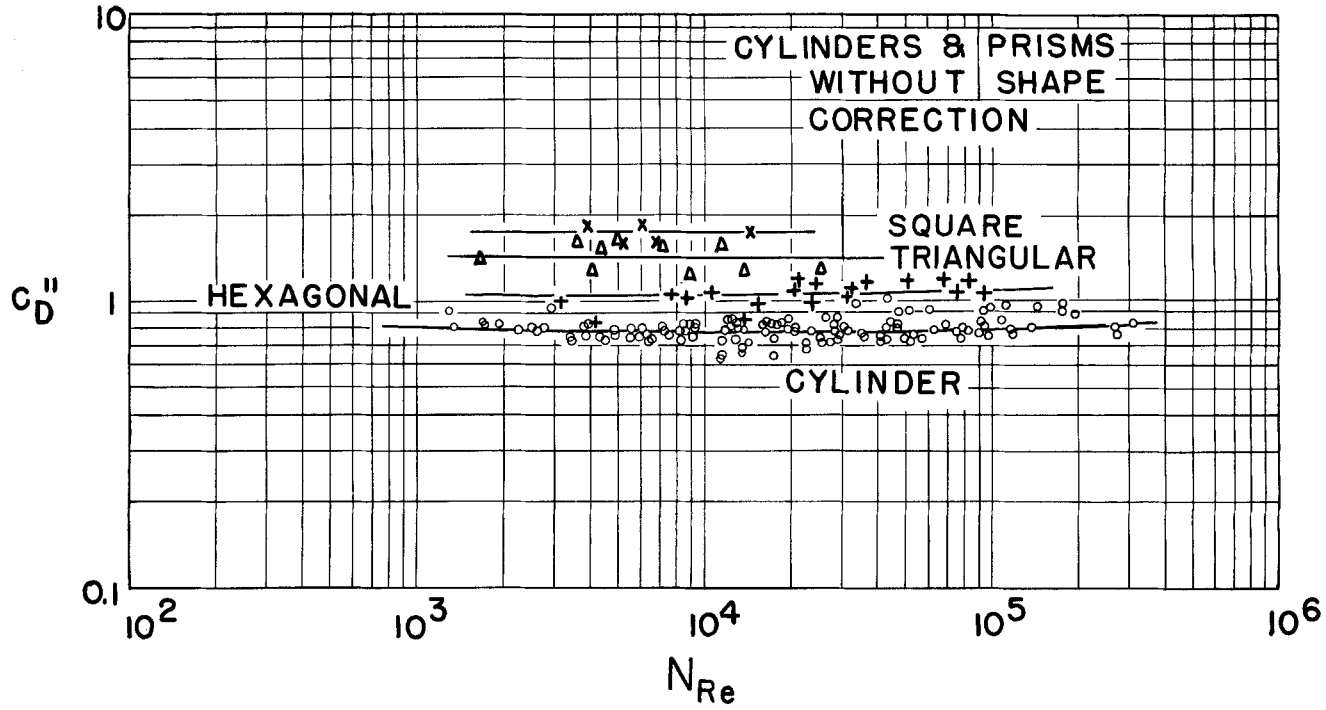

Fig. 2. C''_D vs. N_{Re} for cylinders and prisms in water. $\left[C_D'' = C_D \left(\frac{\rho_p - \rho_f}{\rho_f}\right)^{0.05}\right]$.

eddy shed, an increment of circulation, equal but opposite in sign to that of the eddy, accrues about a body. Consequently, a rotational moment proportional to $\rho_f A u^2 d_{max}$ acts on a body, and, for a free body, this is opposed by an equal moment $I \frac{d\omega}{dt}$. Hence, the ratio $\frac{\rho_f A u^2 d_{max}}{I}$ might be expected to be a criterion which indicates whether a particle will oscillate or rotate and be a measure of the magnitude of oscillation and, to some extent, rotation.

If this ratio is included with the usual flow variables, the following relationship may be obtained by dimensional analysis:

$$C_D \left(\frac{d_{min}}{d_{max}}\right)^m \left(\frac{\rho_p}{\rho_f}\right)^n = f(N_{Re}) \qquad (3)$$

Alternatively, the circulation Γ, developed as discussed above, about a rigid body, especially when the body is spinning, generates a lift force perpendicular to the direction of motion

$$F_L = C_L \rho u \Gamma L = C_L \rho u \omega d^2_{max} L\pi$$

One component of this force opposes the force field and the other acts and induces motion in a direction perpendicular to the force field, hence the oblique or helical path of motion for spinning particles.

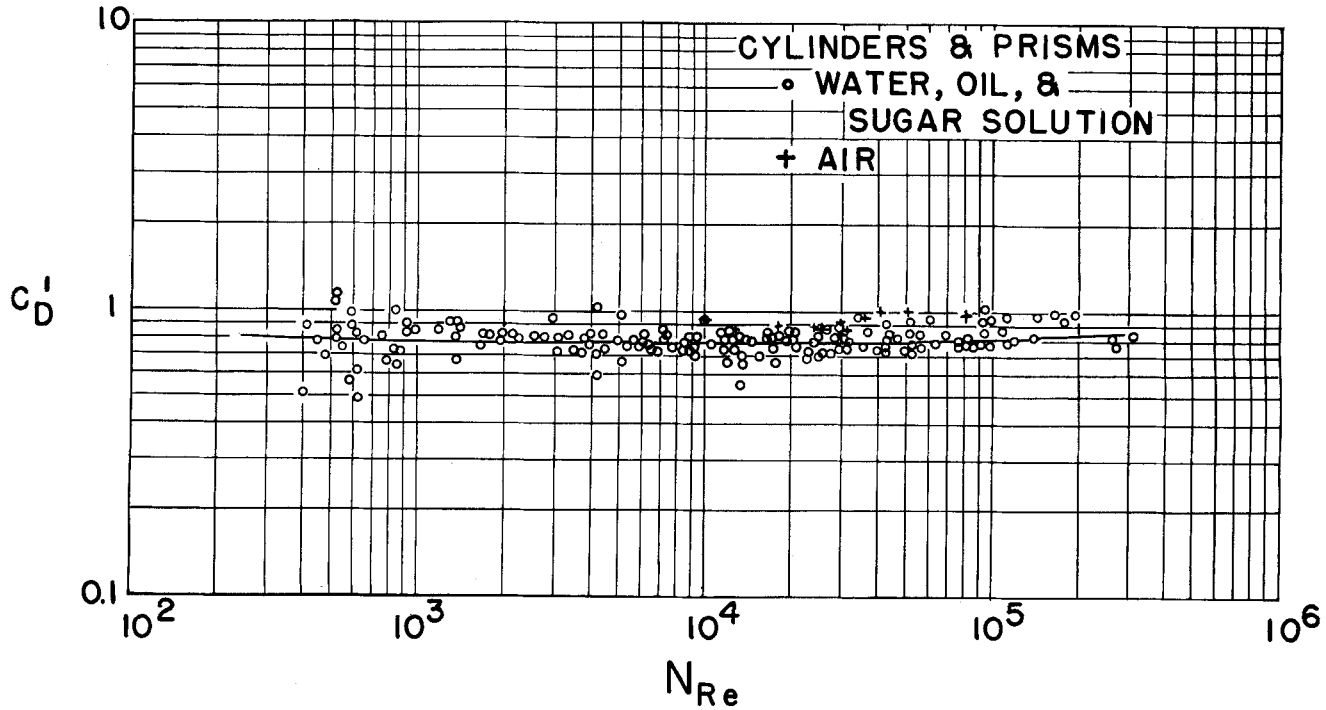

Fig. 3. C'_D computed by Equation (4) vs. N_{Re} for cylinders and prisms in water, aqueous glucose solutions, oil, and air

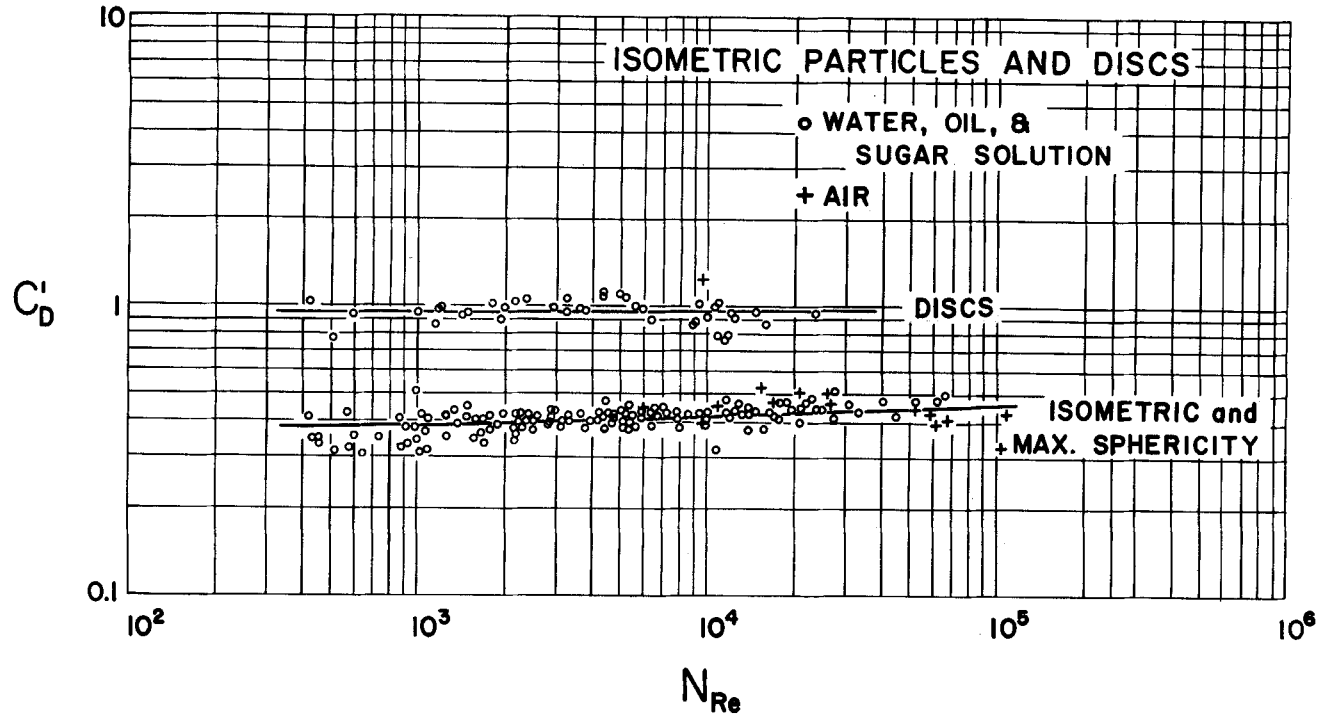

Fig. 4. C'_D, computed by Equation (4), plotted vs. N_{Re} for disks and for isometric and maximum sphericity particles (including spheres) in water, oil, and aqueous glucose solutions and the data of this investigation and Lunnon for spheres in air.

This suggests that the drag coefficient based on motion in the direction of the force field is a function of the ratio of the force of the force field to the lift force:

$$\frac{(\rho_p - \rho_f)Vg}{C_L \rho_f u \omega d^2_{max} L \pi}$$

By inclusion of the variables of this ratio in dimensional analysis, the following relationship may be obtained:

$$C_D \left(\frac{\rho_p - \rho_f}{\rho_f}\right)^{(1+n)} \left(\frac{d_{min}}{d_{max}}\right)^m = f(N_{Re}) = C'_D \quad (4)$$

The data for free fall in water and similar liquids were satisfactorily correlated by either Equation (3) or (4). However, it was found that the data of Lunnon (*15*) and of this investigation for free fall in air could be more satisfactorily correlated with the data for free fall in water by means of Equation (4).

The values of the constants m and n vary slightly with N_{Re} and are unique for each of the three particle classes having characteristic free-fall behavior: cylinders and prisms, disks, and isometric particles. Average values of m and n for Equation (3) for the N_{Re} range of $\sim$ 300 to 10^5 are respectively 2.3 and 1/6 for cylinders and prisms, 0.315 and 1/6 for disks, and 0.0 and 1/18 for isometric particles. Values of m for Equation (4) are identical with those for Equation (3), but n is 0.05 for cylinders, prisms, and disks and 0.03 for isometric particles. Although the values of n are small, the ratios $(\rho_p - \rho_f)/(\rho_f)$ and $(\rho_p)/(\rho_f)$ vary from about 0.2 to 2,800 and 1.2 to 2,800, respectively, and consequently the corrections are in most cases very significant. A complete tabulation of experimental and computed data is given in references *1, 7, 27*.

Typical variation of C_D with particle density for free fall in a fluid, as pointed out earlier, is shown in Figure 1. The variation of C_D with particle shape is indicated in Figure 2, where lines are plotted representing the average drag coefficients corrected for density effect $C_D \left(\frac{\rho_p - \rho_f}{\rho_f}\right)^n$ for cylinders and prisms. The general correlation achieved with Equation (4) for free fall in water, aqueous glucose solutions, oil, and air is shown in Figures 3 and 4. Most of the data are correlated within $\pm$ 10%. Some of the data for $N_{Re} < 1{,}000$ shown in Figures 3 and 4 are transitional flow data and, consequently, deviate considerably from the turbulent flow curve. The data for the isometric and maximum-sphericity particles shown in Figure 4 have been arbitrarily placed on a single line by means of the shape correction factor plotted in Figure 5 as a function of sphericity. The curve was obtained by cross plotting the average values for C'_D vs. the sphericity of each type particle.

An examination of the data of Lunnon (*15*) and of this investigation for free fall in air (Table 1) indicated that if Equation (3) is used, the exponent n is a function of the fluid density. Based on these data, it appears that the value of n should be multiplied by the ratio $\left(\frac{\rho_f}{\rho_{water}}\right)^{1/6}$. With this modification Equation (3) becomes

$$C'_D = \frac{2V}{A} \frac{(\rho_p - \rho_f)g}{\rho_f u^2} \left(\frac{d_{min}}{d_{max}}\right)^m \left(\frac{\rho_p}{\rho_f}\right)^n \left(\frac{\rho_f}{\rho_{water}}\right)^{1/6} \quad (5)$$

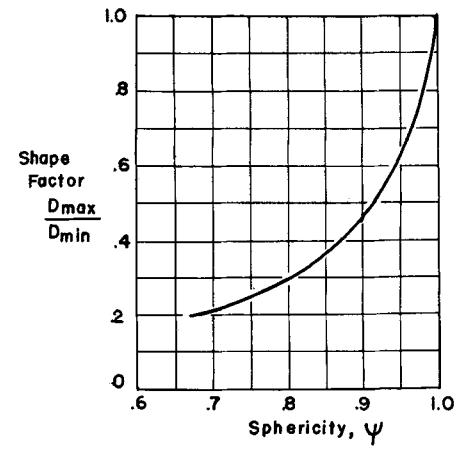

Fig. 5. The shape factor, D_{max}/D_{min} vs. ψ.

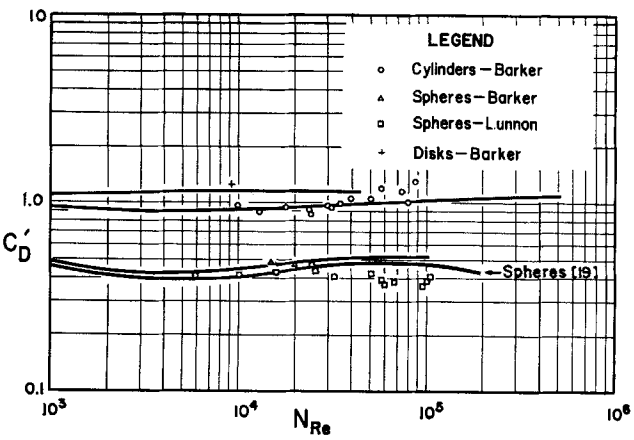

Fig. 6. Average values of C'_D computed by Equation (5) plotted vs. N_{Re} for disks (all cross sections), cylinders (including prisms), and spheres are represented by the curves. The individual data points are for particles in air. The standard plot of C_D vs. N_{Re} for spheres (19) is included for comparison.

When Equation (5) is used, the air data of this investigation agree well with the average curves for free fall in water, as is shown in Figure 6.

The data of Lunnon (*15*) for steel, wood, rubber, wax, and stone spheres falling through air in mine shafts are 15 to 60% lower than the recommended data in the "Chemical Engineers' Handbook" (*19*). Lunnon (*16*) attributed the lowness of some of his data to air motion in the mine shaft. However, if Equation (5) is used, the values for C'_D for the steel spheres (the data considered most reliable by Lunnon and represented in Figure 6 by the data points at $N_{Re} < 30{,}000$) agree with the general curve for spheres.

It will be noted that the correlation of air data by Equation (5) and shown in Figure 6 is somewhat better than that by Equation (4) as shown in Figures 3 and 4, except in the case of the data of Lunnon for spheres at $N_{Re} > 30{,}000$. Also, the correlation based on Equation (5) for all data including air data yields slightly less data scatter than the correlation based on Equation (4). However, Equation (4) is somewhat easier to use than Equation (5), especially in the case of motion in low-density fluids such as gases, and may be found to be equally or more effective when additional and perhaps more reliable data for free fall in air become available and are used in determining the constants. In many engineering calculations involving ordinary liquids, computations with Equation (5) are not particularly difficult since the effect of the exponential fluid density correction is negligibly small and need not be included.

In applying the proposed correlation to particulate motion in fluids, particles are classified as follows. If the ratio of the longest to the shortest distance through a particle is less than 1.7 or if the particle is approximately spherical in general appearance, consider the particle to be isometric. If this ratio is greater than 1.7, consider disklike and elongated particles to be disks and cylinders (or prisms), respectively.

The proposed correlations have not been tested with experimental data for hollow particles or for particles whose volumetric, geometric, and mass centers do not approximately coincide, or whose mass centers do not coincide with the midpoints of the axis. Also, caution should be exercised in applying Equations (4) and (5) to free fall in fluids such as air which have densities differing greatly from the density of water, as it is felt that the air data with which these equations have been tested are incomplete. However, by application to extensive and reliable data (*1, 4, 8*), the correlations have been demonstrated to be valid for liquid densities of 0.8, 1.0, and 1.3 g./cc. and for particle densities varying from 1.2 to 8.3 g./cc.

NOTATION

A = maximum cross-sectional area parallel to the long axis of prisms and cylinders, the cross-sectional area of disks perpendicular to the axis, the projected area of spheres of equal volume for isometric and maximum sphericity particles, sq. cm.
C_D = coefficient of resistance, dimensionless
C'_D = coefficient of resistance modified for the effects of shape and density, dimensionless
C''_D = coefficient of resistance modified for density only, dimensionless
d_{min} = minimum length through the centroid of the maximum projected area parallel to motion and perpendicular to an axis of the cylinder or prism or perpendicular to an axis in the surface of a disk, cm.
d_{max} = minimum length through the centroid of the area described under d_{min}, cm.
d_s = spherical diameter, diameter of a sphere having the same volume as the particle, cm.
d = diameter of cylinder, sphere, or disk, cm.
d_{Re} = characteristic length of the particle to be used in the Reynolds number, cm.
f = function
g = acceleration of gravity, cm./sec.^{2}
L = length of cylinder, cm.
m = exponent for shape correction, dimensionless
n = exponent for density correction, dimensionless
N = number of times a particle was dropped to obtain u, the terminal velocity
R = fluid resistance to particle motion, dynes
N_{Re} = Reynolds number, dimensionless
t = time, sec.
u = relative velocity of the particle with respect to the fluid, cm./sec.
V = volume of the particle, cc.

Greek Letters

ρ_p = density of the particle, g./cc.
ρ_f = density of the fluid, g./cc.
ω = angular velocity, radians/sec.
μ = viscosity of the fluid, poise, g./cm. sec.
ψ = sphericity, the ratio of the surface area of a sphere having the same volume as the particle to the surface area of the particle
Γ = circulation, sq. cm./sec.

LITERATURE CITED

1. Barker, Dee H., Ph.D. thesis, University of Utah, Salt Lake City, Utah (Aug., 1951).
2. Blizzard, I., *J. Franklin Inst.*, **197**, 199-208 (1924).
3. Chowdbury, K. C. R., and W. Fritz, *Chem. Eng. Sci.*, **11**, 92-98 (1959).
4. Christensen, J. J., Jr., M.S. thesis, University of Utah, Salt Lake City, Utah (Aug., 1955).
5. Christiansen, E. B., Ph.D. thesis, University of Michigan, Ann Arbor, Michigan (July, 1943).
6. ———, and Dee H. Barker, *Rev. Sci. Inst.*, **23**, 427-430 (1952).
7. ———, *Tech. Bull. No. 1*, Dept. of Chem. Eng., University of Utah, Salt Lake City, Utah (Feb., 1963).
8. Christiansen, E. B., Unpublished data for cylinders, disks, and prisms taken at the University of Michigan; see reference *1*, p. 162.

9. Duplieh, P., *Natl. Advisory Comm. Aeronaut. Tech. Note 1201* (1949)
10. Heiss, J. F., and J. Coull, *Chem. Eng. Progr.*, **48**, 133 (1952).
11. Heywood, H., *Proc. Inst. Mech. Engrs. (London)*, **140**, 257 (1938).
12. Krumbein, W. C., *Am. Geophysical Union*, 621-632 (1942).
13. Langhaar, Henry L., "Dimensional Analysis and Theory of Models," pp. 13-20, Wiley, New York (1951).
14. Liebster, H., *Ann. Physik*, **82**, 541-62 (1927).
15. Lunnon, R. G., *Proc. Roy. Soc. (London)*, **A110**, 302-36 (1926).
16. Ibid., **A118**, 680-94 (1928).
17. McNown, J. S., and Jamil Malaika, *Trans. Am. Geophysical Union*, **31**, 74-82 (1950).
18. Pernolet, V., *Annales Des Mines 4me Sines*, **20**, 379 and 535 (1851).
19. Perry, J. H., "Chemical Engineers Handbook," 3 ed., 1019, McGraw-Hill, New York (1950).
20. Pettyjohn, E. S., and E. B. Christiansen, *Chem. Eng. Progr.* **44**, 157-72 (1948).
21. Richards, R. H., *Trans. Am. Inst. Mining, Met. Engrs.*, 38, 210-35 (1908).
22. Schmiedel, J., *Physik. Z.*, **29**, 594-610 (1928).
23. Squires, L., and W. J. Squires, *Trans. Am. Inst. Chem. Engrs.*, **33**, 1 (1937).
24. Stokes, G. G., *Trans. Cambridge Phil. Soc.*, **9**, Part II, p. 51 (1851).
25. Wadell, H., *J. Franklin Inst.*, **217**, 459-67 (1934).
26. Willmarth, W. W., N. E. Hawk, and R. L. Harvey, *Phys. Fluids*, **7**, 197-208 (1964).
27. Tabular material has been deposited as document with the American Documentation Institute, Photoduplication Service, Library of Congress, Washington 25, D. C. as Document number 8175 and may be obtained for $7.50 for photoprints or $2.75 for 35-mm. microfilm.

Manuscript received May 24, 1963; revision received September 25, 1964; paper accepted September 28, 1964. Paper presented at A.I.Ch.E. Atlanta meeting.

Analysis of Phase Boundary Motion in Diffusion-Controlled Processes: Part II. Application to Evaporation from a Flat Surface

J. R. GRIFFIN and D. R. COUGHANOWR

Purdue University, Lafayette, Indiana

In an earlier paper (*1*), three general methods of approaching the moving-boundary problems were developed. In the present work, these three methods are applied in detail to the solution of the problem of evaporation from a flat surface into a vapor phase of infinite depth. While this particular problem has been solved before (*2,3*), it has been chosen as an example here because all three methods apply directly.

DESCRIPTION OF PROBLEM

A liquid evaporates from a large, flat surface into a vapor region which may be considered to extend an infinite distance above the interface. The vapor consists of the diffusant and a gas, such as air, which is insoluble in the liquid. The process is assumed to be controlled by mass diffusion of the evaporated species through the vapor. The evaporating species is the only transferred matter, and the initial concentration in the gas is uniform. The concentration levels and phase density difference are such that the motion of the vapor phase away from the surface cannot be ignored. It is desired to find an equation for the phase boundary motion.

The differential equation accounting for the bulk motion is given by Equation (I.38):*

$$D\frac{\partial^2 w}{\partial x^2} - \epsilon \dot{X}\frac{\partial w}{\partial x} = \frac{\partial w}{\partial \theta} \qquad (1)$$

The initial conditions are

$$w = w_o \qquad \theta = 0 \qquad (2)$$
$$X = X_o$$

J. R. Griffin is with the Humble Oil and Refining Company, Baytown, Texas.

* The Roman numeral preceding an equation number refers to an equation in Part I of this series of papers (*1*). The form taken by Equation (1) involves a number of assumptions, such as constant phase densities and diffusivity.